J. Ind. Geophys. Union, 29(1) (2025), 45-55

Finite Element solutions of Maxwell fluid flow towards a stretching surface with addition of thermal radiation, porous medium and magnetic field

Nagaraju Bathula* and Kishan Naikoti
Department of Mathematics, Osmania University, Hyderabad-500007, Telangana, India.
*Corresponding author: bnag2014@gmail.com

ABSTRACT

Numerical simulations were used to study the flow of a Maxwell fluid across a non-linear stretching sheet. The effects of thermal radiation, magnetic field, and porous media, were all taken into account within the parameters of the experiment. The non-linear governing equations and the associated boundary conditions were solved using an approach called the finite element technique. Several technical features were used to examine the effects of various factors on the temperature, concentration, and velocity profiles. This study considered parameters like, the magnetic field , permeability , non-linear stretching sheet, Prandtl number, and the thermal radiation. The study also examines the graphical depictions of how the physical elements affect the skin-friction coefficients along the x and y - directions and heat transfer rate. This was done in tandem with the findings, which are shown graphically.

Keywords: Maxwell fluid; Magnetic field; Thermal radiation; Porous medium; Finite element metho

INTRODUCTION

Fluids play a critical role in numerous industrial processes, with non-Newtonian fluids exhibiting particularly unique rheological properties. Applications such as plastic sheet extrusion, paper manufacturing, metal spinning, and glass fiber production, exemplify the widespread use of these materials. Maxwell's model, a cornerstone of non-Newtonian fluid theory, provides a framework for predicting stress relaxation behavior in these complex systems. Furthermore, magnetohydrodynamics (MHD) elucidates the interaction between magnetic fields and electrically conductive fluids in motion. This interaction generates forces within the fluid, enabling novel control mechanisms and applications in various industrial settings.

Sandeep and Sulochana (2018) conducted a comprehensive investigation into the stretching surface flows of Oldroyd-B, Jeffrey, and Maxwell fluids, considering the effects of nonuniform heat source/sink perturbations and radiation. In a subsequent study, Farooq et al. (2019) delved into the exponentially expanding sheet flow of Maxwell-type nanomaterials. Wang et al. (2019) and Sun et al. (2019) developed a model for incompressible Maxwell fluid flow through a tube with a triangular cross section, which could be either rectangular or isosceles. The unsteady flow of viscoelastic fluid with a fractional Maxwell model in a channel, was investigated by Haitao and Mingyu (2007). Wenchang et al. (2003) utilized the fractional Maxwell model to investigate the unsteady flows of a viscoelastic fluid between two parallel plates. Qi and Liu (2011) explored analogue duct flows of a fractional Maxwell fluid. On the other hand, Saleem et al. (2017) examined the 3D mixed convective Maxwell fluid, using mass and heat Catteneo-Christov heat flow models, while considering heat production. Similarly, Fetecau and Fetecau (2003) discovered an exact numerical solution for fluid flow in Maxwell's law.

Apart from the above studies , the propagation of Maxwell fluid in a porous medium was studied by Wang and Hayat (2008) and the behaviour of fraction Maxwell fluid in unsteady flow was investigated by Fetecau et al. (2014). A two-dimensional magnetohydrodynamic (MHD) Maxwell fluid was also studied by Hayat et al. (2009). Similarly, Heyhat and Khabzi (2011) investigated the upper-convicted Maxwell (UCM) fluid flow across a flat rigid region in a magnetohydrodynamic (MHD) system and series solutions for two-dimensional magnetohydrodynamic circulation with thermophoresis and Joule heating, were obtained by Hayat and Qasim (2010). Similarly, Jamil and Fetecau (2010) studied Maxwell fluid in relation to helical flows between coaxial cylinders. Zheng et al. (2011) found exact mathematical solutions for a rotating flow model based on a generalized Maxwell fluid. To better understand how Maxwell fluid behaves in the presence of porous media, double-diffusive convection, and Soret effects, Wang and Tan (2011) also undertook a stability study. Sivaiah et al. (2012a,b,c) modeled and analyzed heat and mass transfer effects on unsteady MHD convection flow via finite element method. Motsa et al. (2012) examined the UCM flow in a porous structure. Reddy et al. (2012) too studied heat and mass transfer effects on unsteady MHD free convection flow past a vertical permeable moving plate with radiation. Further, the dynamics of thermally radiative Maxwell fluid flow over a continuously permeable expanding surface were characterized by Mukhopadhyay et al. (2013). Ramesh et al. (2017) too examined the Maxwell fluid with nanomaterials for magnetohydrodynamic (MHD) flow in a Riga plate computationally. In addition to above mentioned studies, Deepa and Murali. (2014) and Deepa and Gundagani (2014) analyzed the viscous dissipation, soret and dufour effects on unsteady MHD flow using finite difference method.

In the realm of magnetohydrodynamic (MHD) driven systems, the finite element solutions found by Murali et al. (2023) and Murali and Babu (2023) represented a significant advancement. The comprehension of these solutions was greatly enriched by the foundational research of Babu et al. (2015, 2018), whose seminal works are meticulously cited throughout the literature. Besides, heat and mass transfer effects were studied by a large number of researchers like Singh et al. (2023), Gundagani et al. (2012, 2013a,b, 2024a,b), Tanuku et.al (2024), Gundagani and Babu (2012) and Murali et al. (2015a,b). The interplay of these scholarly contributions has undeniably propelled the field forward, offering a robust framework for future explorations and applications within the domain of MHD systems.

An analysis is presented here on the magnetohydrodynamic (MHD) flow of a non-Newtonian, non-viscous Maxwell fluid via a stretched surface in a porous medium, considering the influence of heat radiation. Non-linear ordinary differential equations are solved using the finite element treatment. The temperature, velocity (in the *x* and *y*-directions), and profiles are examined by the use of graphs derived from the solutions obtained by the finite element method. Data on the Skin-friction coefficients in the *x* and *y* directions, along with the local Nusselt number, are analyzed using tabular representations. The obtained findings show a high level of concordance with past data in comparison to currently available data.

MATHEMATICAL FORMULATION

In this section, the effects of thermal radiation and magnetic field on three-dimensional, steady, incompressible, viscous, non-Newtonian Maxwell fluid flow, past a stretching surface embedded in porous medium, has been dealt. The geometry of the fluid flow is shown in Figure 1. To undertake this inquiry, the following premises are assumed:

i. The magnetic Reynolds number is considered as low as possible to neglect the induced magnetic field.

ii. The velocities of the sheet along the *x* - and *y* - directions are assumed to be U_w (x) = ax and V_w (y) = by respectively.

iii. A magnetic field of strength B_o is applied to the flow.

iv. In energy equation, Ohmic heating, Thermophoresis, Brownian motion, Viscous dissipation, Diffusion thermo, Heat source and Joule heating effects are neglected.

v. Let T_w be the constant temperature at the sheet, whereas T_∞ denotes the fluid temperature outside the thermal boundary layer.

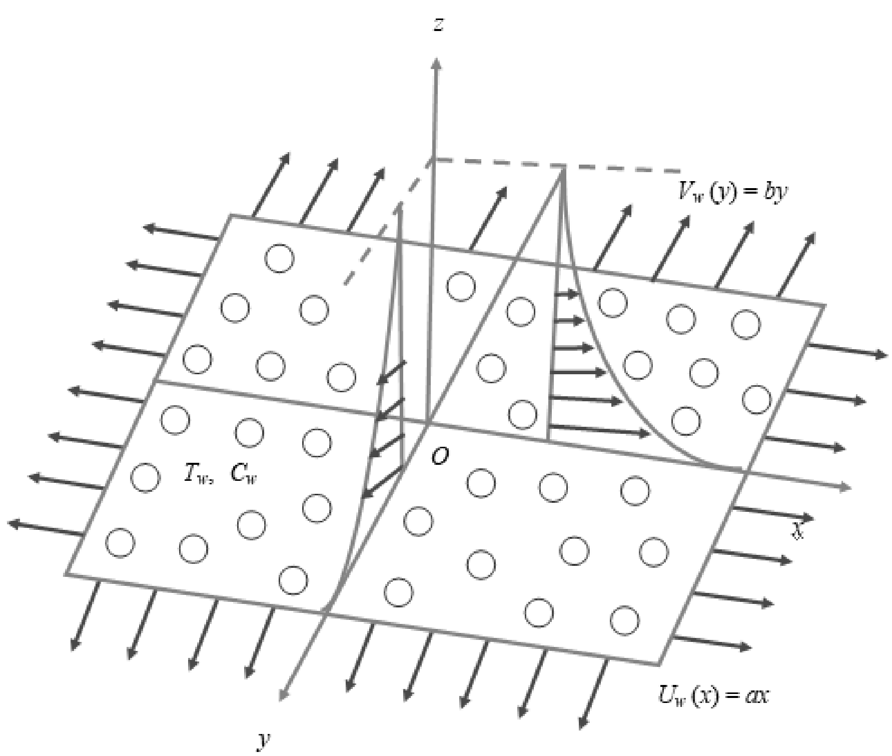

Figure 1. Geometrical representation of Maxwell fluid flow

Based on the above assumptions, the basic governing equations for Maxwell-Nanofluid flow are,

Continuity Equation:

$$\frac{\partial u}{\partial x}+\frac{\partial v}{\partial y}+\frac{\partial w}{\partial z}=0 \tag{1}$$

Momentum Equation:

$$u(u_x)+v(u_y)+w(u_z)+\lambda\left[u^2(u_{xx})+v^2(u_{yy})+w^2(u_{zz})+2uv(u_{xy})+2vw(u_{yz})+2uw(u_{xz})\right]=u_{zz}-(\frac{v}{k^*})u-[\frac{\sigma(B_o)^2}{\rho}]u \tag{2}$$

$$u(v_x)+v(v_y)+w(v_z)+\lambda\left[u^2(v_{xx})+v^2(u_{yy})+w^2(u_{zz})+2uv(v_{xy})+2vw(v_{yz})+2uw(v_{xz})\right]=v_{zz}-(\frac{v}{k^*})u-[\frac{\sigma(B_o)^2}{\rho}]v \tag{3}$$

Equation of thermal energy:

$$u\left(\frac{\partial T}{\partial x}\right)+v\left(\frac{\partial T}{\partial y}\right)+w\left(\frac{\partial T}{\partial z}\right)=\alpha\left(\frac{\partial^2 T}{\partial z^2}\right)-\frac{1}{\rho C_p}\left(\frac{\partial q_r}{\partial z}\right) \tag{4}$$

The boundary conditions for this flow are

$$u=U_w=ax,\ v=V_w=by,\ w=0,\ T=T_w\ \ at\ \ z=0\ \&\ u\to 0,\ v\to 0,\ T\to T_\infty\ \ as\ \ z\to\infty \tag{5}$$

The radiative heat flux q_r (using Roseland approximation) is defined as

$$q_r=-\frac{4\sigma^*}{3K^*}\left(\frac{\partial T^4}{\partial z}\right) \tag{6}$$

We assume that the temperature variances inside the flow are such that the term T^4 can be represented as linear function of temperature. This is accomplished by expanding T^4 in a Taylor series about a free

stream temperature T_∞ as follows:

$$T^4=T_\infty^4+4T_\infty^3\left(T-T_\infty\right)+6T_\infty^2\left(T-T_\infty\right)^2+\ldots\ldots\ldots\ldots \tag{7}$$

After neglecting higher-order terms in the above equation beyond the first-degree term in $\left(T-T_\infty\right)$, we get

$$T^4\cong 4T_\infty^3 T-3T_\infty^4 \tag{8}$$

Thus substituting Eq. (8) in Eq. (6), we get

$$q_r=-\frac{16T_\infty^3\sigma^*}{3K^*}\left(\frac{\partial T}{\partial z}\right) \tag{9}$$

Using (9), Eq. (4) can be written as

$$u\left(\frac{\partial T}{\partial x}\right)+v\left(\frac{\partial T}{\partial y}\right)+w\left(\frac{\partial T}{\partial z}\right)=\alpha\left(\frac{\partial^2 T}{\partial z^2}\right)+\frac{1}{\rho C_p}\left(\frac{16T_\infty^3\sigma^*}{3\kappa k^*}\right)\left(\frac{\partial^2 T}{\partial z^2}\right) \quad 10)$$

Initiating the following similarity transformations

$$\eta=\left(\sqrt{\frac{a}{\nu}}\right)z,\ \ u=axf'(\eta),\ v=ayg'(\eta),\ \ \theta=\frac{T-T_\infty}{T_w-T_\infty},\ w=\nu\sqrt{\nu a}\left\{f(\eta)+g(\eta)\right\} \tag{11}$$

Making use of Eq. (11), equation of continuity (1) is identically satisfied and Eqs. (2), (3), and (10) take the following form

$$f'''-f'^2+ff''+gf''-Mf'+K\left\{2ff'f''+2gf'f''-\left(f+g\right)^2f'''\right\}-\delta f'=0 \tag{12}$$

$$g'''-g'^2+fg''+gg''-Mg'+K\left\{2fg'g''+2gg'g''-\left(f+g\right)^2g'''\right\}-\delta f'=0 \tag{13}$$

$$\left\{\frac{d}{d\eta}\left[\left(1+R\left(1+\left(\theta_w-1\right)\theta\right)^3\right)\theta'\right]\right\}+\Pr f\theta'+\Pr g\theta'=0 \tag{14}$$

the corresponding boundary conditions (5) becomes

$$f(0)=0,\ g(0)=0,\ f'(0)=1,\ g'(0)=C,\ \theta(0)=1,\ f'(\infty)\to 0,\ g'(\infty)\to 0,\ \theta(\infty)\to 0 \tag{15}$$

where the involved physical parameters are defined as

$$M=\frac{\sigma B_o^2}{\rho U_o},\ K=\lambda_1 a,\ \ C=\frac{b}{a},\ \ \theta_w=\frac{T_w}{T_\infty},\ \Pr=\frac{\nu}{\alpha},\ R=\frac{16\sigma^* T_\infty^3}{3\kappa k^*},\ \ \delta=\frac{\nu}{aK_o} \tag{16}$$

Quantities of physical interest, the physical parameters of the skin-friction coefficient along x and y - directions, local Nusselt number are presented as follows:

$$C_{fx}=\frac{\tau_{wx}}{\rho U_w^2}=\frac{1}{\rho U_w^2}\mu\left(\frac{\partial u}{\partial y}\right)_{y=0}\Rightarrow Cfx=C_{fx}\left(\sqrt{\mathrm{Re}_x}\right)=f''(0) \tag{17}$$

$$C_{fy}=\frac{\tau_{wy}}{\rho V_w^2}=\frac{\mu}{\rho V_w^2}\left(\frac{\partial v}{\partial y}\right)_{y=0}\Rightarrow Cfy=C_{fy}\left(\sqrt{\mathrm{Re}_y}\right)=g''(0) \tag{18}$$

$$Nu=\frac{xq_w}{\kappa\left(T_w-T_\infty\right)}=-\frac{x\left(\frac{\partial T}{\partial y}+\frac{\partial q_r}{\partial y}\right)_{y=0}}{\kappa\left(T_w-T_\infty\right)}\Rightarrow Nu=-\left(1+R\theta_w^3\right)\left(\sqrt{\mathrm{Re}_x}\right)\theta'(0) \tag{19}$$

Where $\mathrm{Re}_x=\frac{U_w x}{\nu}$ is local Reynolds number based on the stretching velocity U_w (x) and $\mathrm{Re}_y=\frac{V_w y}{\nu}$ is local Reynolds number based on the stretching velocity V_w (y).

METHOD OF SOLUTION

Numerous numerical techniques, including as the LU decomposition approach, the Gauss elimination method, and others, can be used to solve built equations. It is crucial to keep in mind the form functions used to approximately approximate real functions while working with real numbers. The flow domain is made up of 10,000 identically sized quadratic components and a total of 20,001 nodes. 10,000 quadratic components of identical size make up the flow domain. We were given 80,04 nonlinear equations to research after constructing the fundamental equations. The remaining system of nonlinear equations is then numerically solved with a precision of 0.00001 using the Gauss elimination method, once the boundary conditions have been applied. The use of Gaussian quadrature makes integrates solutions easier. The method's computer software was written in the MATHEMATICA programming language and executed on a desktop machine.

PROGRAM CODE VALIDATION

The validation of present numerical results is compared with the published results of Mushtaq et al. (2016) in Table 1 in absence of magnetic field and porous medium effects for various values of C at Pr = 1.0. From this table, it is observed that, the present results are in very good agreement with their results.

RESULTS AND DISCUSSION

In the previous section, the set of ordinary differential equations (12), (13) and (14) are solved using the finite element method with the help of boundary equations (12). In this section, we demonstrate the effects of various parameters such as M = 0.5, K = 0.5, C = 0.5, Pr = 0.22, R= 0.5, and δ = 0.1, θ_w = 0.5 on velocity (velocity components along the x - and y - axes) and temperature profiles (Figures 2-12). Also, the numerical values of Skin-friction coefficients along x - and y - axes and rate of heat transfer coefficient with the same parameter variations are discussed in Tables 2, 3 and 4 respectively.

Figures 2 and 3 show the effect of magnetic field parameter (M) on velocity profiles along x - and y - directions respectively. It has been shown that the velocity fields diminish as the value of M rises. The fluid flow tends to slow down in the presence of a magnetic field. The influence of Maxwell fluid parameter or Deborah number (K) on the x - and y - components of velocity is sketched in the Figures 4 and 5 respectively. The fluid's relaxation period's deviation from its basic time scale is quantified by the Deborah number. The relaxation period is the amount of time the fluid requires to reach equilibrium following the application of the shear force. It is anticipated that fluids with a higher viscosity may take longer to relax.

Table 1. Validation of present numerical results with the published results of Mushtaq et al. (2016) for different values of C at Pr = 1.0 when M = 0, and δ = 0.

C	Present numerical results			Obtained by Mushtaq et al. (2016)		
	$-f''(0)$	$-g''(0)$	$-\theta'(0)$	$-f''(0)$	$-g''(0)$	$-\theta'(0)$
0.25	1.0256378487	0.1181027022	0.6515670171	1.048811	0.194564	0.665926
0.50	1.0859659654	0.4526534797	0.7234146547	1.093095	0.465205	0.735333
0.75	1.1287554899	0.7865763453	0.7753675487	1.134486	0.794618	0.796472
1.00	1.1645765434	1.1609873546	0.8409867124	1.173721	1.173721	0.851992

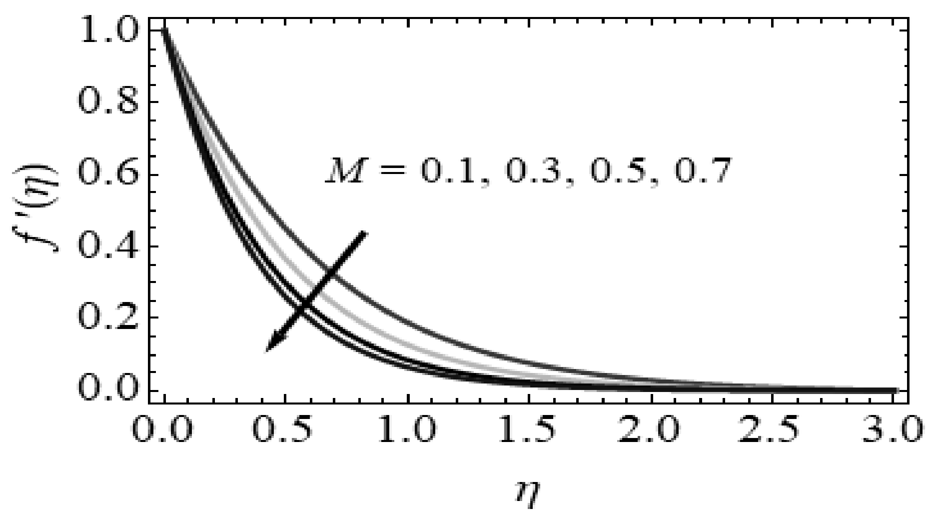

Figure 2. Primary velocity profiles (f') for different values of Magnetic field parameter (M)

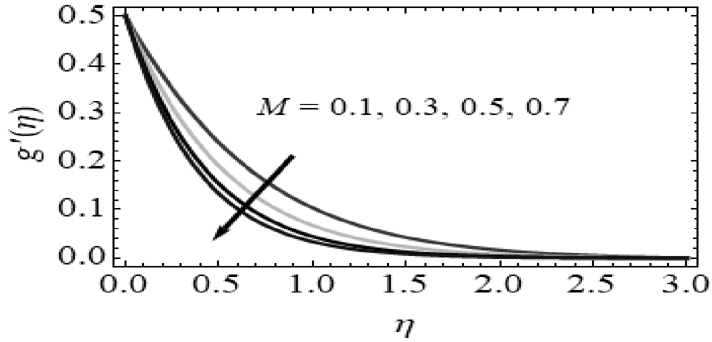

Figure 3. Secondary velocity profiles (g') for different values of Magnetic field parameter (*M)*

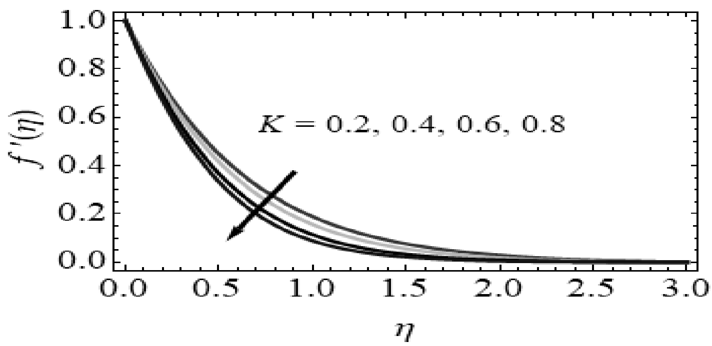

Figure 4. Primary velocity profiles (*f ')* for different values of Maxwell fluid parameter (*K)*

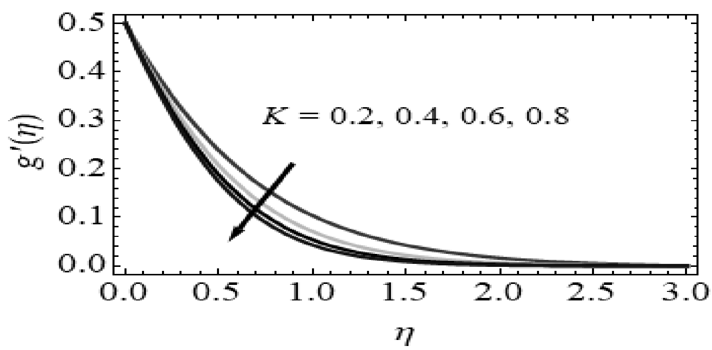

Figure 5. Secondary velocity profiles(g') for different values of Maxwell fluid parameter (*K)*

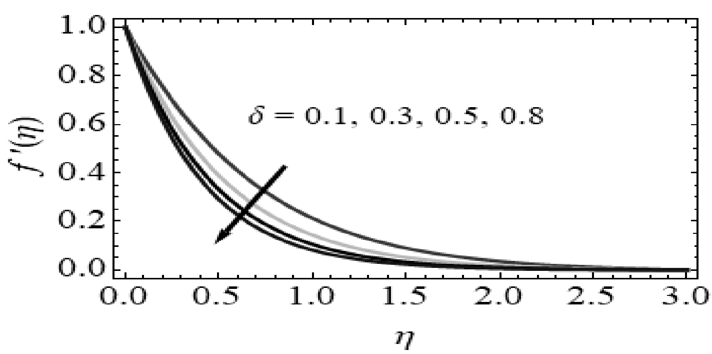

Figure 6. Primary velocity profiles (*f ')* for different values of permeability parameter (δ)

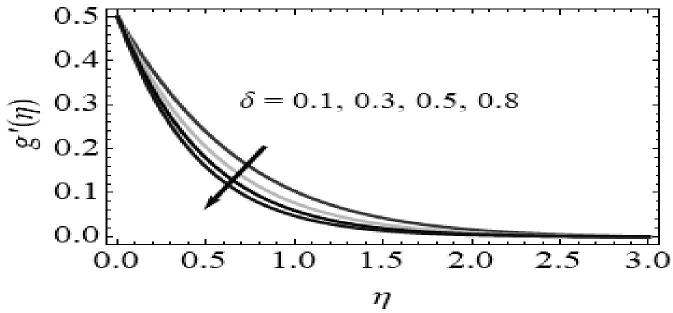

Figure 7. Secondary velocity profiles(g') for different values of permeability parameter (δ)

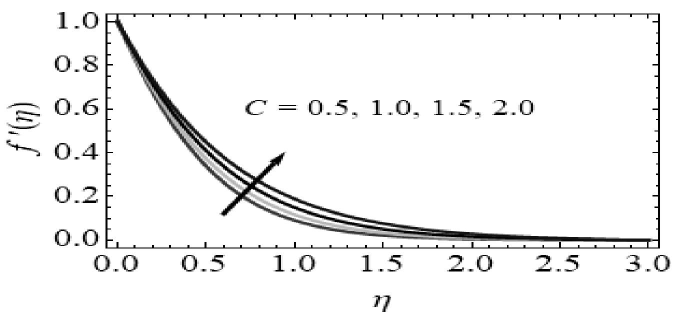

Figure 8. Primary velocity Profiles **(**f'*)* for different values of velocity ratio parameter (C)

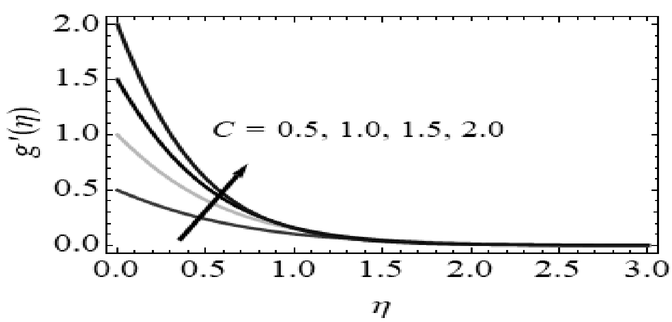

Figure 9. Secondary velocity profiles(g') for different values of velocity ratio parameter (C)

It is possible to interpret an increase in K in this way because fluid viscosity restricts fluid motion and lowers velocity. As a result, the hydrodynamic boundary layer thins when K is increased. It is also noted that change in the velocity fields f' and g' is larger in the three-dimensional flow when compared with the two-dimensional and axi-symmetric flows. Figures 6 and 7 illustrate the effect of permeability parameter (δ) on the velocity distributions along x - and y - directions respectively. From these figures, it is observed that the velocity profiles decreases with the increase in permeability (porosity) parameter K. This arises because an increase in K amplifies the porous layer and thereby reduces the thickness of momentum boundary layer.

Figures 8 and 9 show the behaviour of velocity ratio parameter (C) on primary and secondary velocity profiles respectively. From these figures, it is observed that, both the primary and secondary velocity profiles increase with rising values of velocity ratio parameter. The variation of Prandtl number on temperature outlines is shown in Figure 10. It is concluded that increasing values of Prandtl number result in a thinner temperature boundary layer thickness. Fluids having larger Prandtl number have lower thermal diffusivity, and hence the temperature decreases. Figure 11 shows the variation that are seen in temperature profiles due to increase in the values of (R). Because the conduction effect of the nanofluid increases in the presence of R, it is noticed that the fluid temperature rises as R increases. Higher values of R thus imply higher surface heat flow, which raises the temperature in the boundary layer area.

Figure 12 includes the behaviour of temperature ratio parameter θ_w on the temperature distribution. Bigger values of θ_w corresponds to a larger temperature and thicker thermal boundary layer.

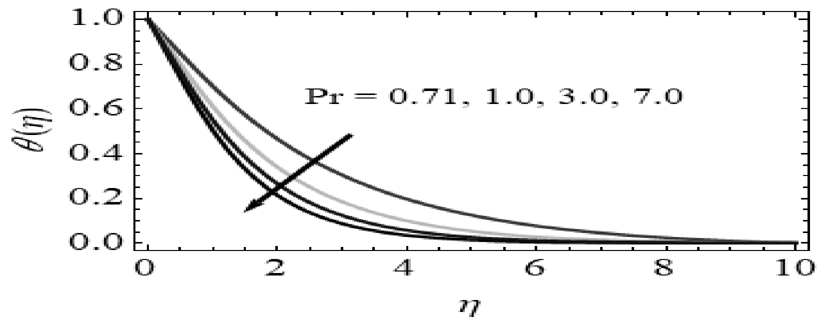

Figure 10. Temperature profiles for different values of Prandtl number (Pr)

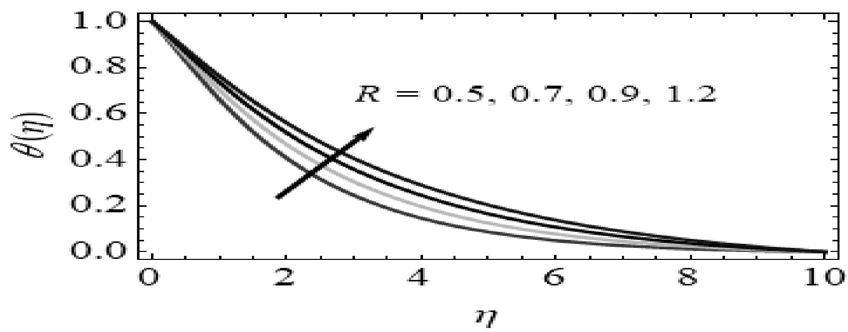

Figure 11. Temperature profiles for different values of thermal radiation parameter (*R)*

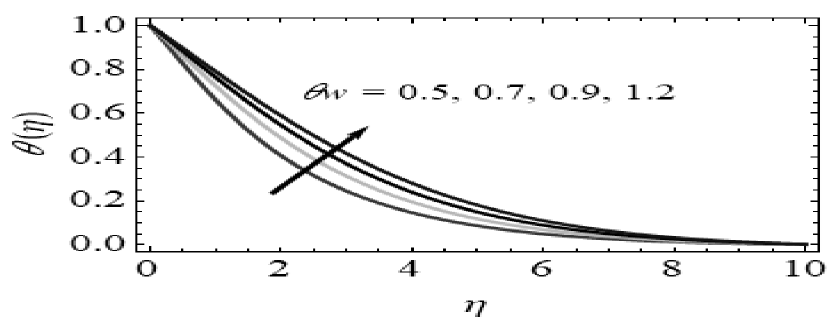

Figure 12. Temperature profiles for different values of temperature ratio parameter(θw)

This is explained as follows. It is clear from energy Eq. (14) that effective thermal diffusivity is the sum of classical thermal diffusivity (α) and thermal diffusivity due to the radiation effect. Thus one anticipates that parameter θ_w, being the coefficient of the later term, would support the thermal boundary layer thickness. It can be further noticed that the profiles attain special *S*-shaped form when θ_w enlarges, which dictates the existence of adiabatic case. In other words, the wall temperature gradient approaches zero value when wall to ambient temperature ratio is sufficiently large.

The numerical values of various parameters namely, *M*, *K*, *C*, δ, Pr, *R*, θ_w on Skin-friction coefficients along *x* - (*Cfx*) and *y* - (*Cfy*) directions are discussed in Tables 2 and 3 respectively. From these tables, it is observed that, the Skin-friction coefficients along *x* - (*Cfx*) and *y* - (*Cfy*) directions are increasing with increasing values of *C*, *R*, θ_w and is decreasing with increasing values of *M*, *K*, and Pr. From these tables, it is observed that, the Skin-friction coefficients along *x* - (*Cfx*) and *y* - (*Cfy*) directions are increasing with increasing values of *C*, *R*, θ_w and is decreasing with increasing values of *M*, *K*, and Pr. The tabular values of rate of heat transfer coefficient or Nusselt number (*Nu*) for different values of Pr, *R*, and θ_w are shown in Table 4. From this table, it is observed that, the rate of heat transfer coefficient is increasing with rising values of *R*, θ_w, and opposite effect is observed with the effect of Pr.

Table 2. Results of Skin-friction coefficient along *x*-direction

M	K	δ	C	Pr	R	θ_w	Cfx
0.1	0.2	0.1	0.5	0.71	0.5	0.5	3.5667620975
0.3							3.5014748743
0.5							3.4867190992
	0.4						3.5153646203
	0.6						3.4714674308
		0.3					3.5125675082
		0.5					3.4956748481
			1.0				3.5966573450
			1.5				3.6145780621
				1.00			3.5045465823
				3.00			3.4714665621
					0.7		3.5856187502
					0.9		3.6064720278
						0.7	3.5856586580
						0.9	3.6036465591

Table 3. Results of Skin-friction coefficient along *y*-direction

M	K	δ	C	Pr	R	θ_w	Cfy
0.1	0.2	0.1	0.5	0.71	0.5	0.5	2.7590650945
0.3							2.7254704872
0.5							2.6947557921
	0.4						2.7215627057
	0.6						2.6945469252
		0.3					2.7105657871
		0.5					2.6845586825
			1.0				2.7857501722
			1.5				2.8045252876
				1.00			2.7156706702
				3.00			2.6835456924
					0.7		2.7845645923
					0.9		2.8056756108
						0.7	2.7756701011
						0.9	2.7956750572

Table 4. Rate of heat transfer coefficient results

Pr	R	θ_w	Nu
0.71	0.5	0.5	1.8548832158
1.00			1.8113760176
3.00			1.7859060651
	0.7		1.8838604560
	0.9		1.9075789431
		0.7	1.8945457965
		0.9	1.9036460934

The tabular values of rate of heat transfer coefficient or Nusselt number (Nu) for different values of Pr, R, and θ_w are shown in Table 4. From this table, it is observed that, the rate of heat transfer coefficient is increasing with rising values of R, θ_w, and opposite effect is observed with the effect of Pr.

CONCLUSIONS

The present study investigates the combined impact of heat radiation and magnetic field on a stable, two-dimensional, incompressible, viscous, non-Newtonian Maxwell fluid flowing towards a stretched sheet in the presence of a porous material. The fundamental partial differential equations are used to represent the present problem prior to their transformation into ordinary differential equations. Next, the finite element approach is used to numerically solve these equations. Hence, it is feasible to analyze and communicate the velocity and temperature patterns graphically. Key aspects of this effort are:

i. The velocity profiles along *x* - and *y* - directions decrease with increasing values of Maxwell fluid parameter, magnetic field parameter, permeability parameter, and the reverse effect is observed in the case of velocity ratio parameter.
ii. The temperature profiles show increasing trend with increasing values of thermal radiation parameter, and temperature ratio parameter while reverse effect is observed in the case of Prandtl number.
iii. Finally, the present numerical results are very good agreement with the published results of Mushtaq et al. (2016).

List of Symbols:

u, v, w **:** Velocity components in *x*, *y* and *z*axes respectively (*m*/*s*)
x, y, z **:** Cartesian coordinates measured along the stretching sheet (*m*)
f **:** Dimensionless stream function along *x* - direction (*kg* / *m. s*)
f' **:** Fluid velocity along *x* - direction(*m*/*s*)
K_o**:** Dimensional Permeability parameter
g **:** Dimensionless stream function along *y* - direction (*kg* / *m. s*)
g' **:** Fluid velocity along *y* - direction(*m*/*s*)
Pr**:** Prandtl number
*T***:** Fluid temperature (*K*)
T_∞ **:** Temperature of the fluid far away from the stretching sheet (*K*)
Cf_x **:** Skin-friction coefficient along *x* - direction (s^{-1})
Cfx **:** Non-dimensional skin-friction coefficient along *x* - direction (s^{-1})
M **:** Magnetic field parameter
B_o **:** Uniform magnetic field (*Tesla*)
a, b **:** Constants
T_w **:** Temperature at the surface (*K*)
O **:** Origin
K **:** Maxwell fluid parameter
R **:** Thermal radiation parameter
q_r **:** Radiative heat flux
Cf_y **:** Skin-friction coefficient along *y* - direction (s^{-1})
Cfy **:** Non-dimensionalSkin-friction coefficient along *y* - direction (s^{-1})
$U_w(x)$ **:** Stretching velocity of the fluid along *x* - direction (*m*/*s*)
$V_w(y)$: Stretching velocity of the fluid along *y* - direction (*m*/*s*)
q_w **:** Heat flux coefficient
Nu **:** Rate of heat transfer coefficient (or) Nusselt number
C_p **:** Specific heat capacity of nano particles (*J / kg / K*)
C **:** Stretching sheet parameter
Re_x **:** Reynolds number along *x* - direction
Re_y **:** Reynolds number along *y* - direction
K^* **:** Mean absorption coefficient

Greek symbols:

η **:** Dimensionless similarity variable (*m*)
θ **:** Dimensionless temperature (*K*)
ν **:** Kinematic viscosity (m^2 / s)
σ **:** Electrical Conductivity
ρ **:** Fluid density (kg / m^3)
κ **:** Thermal conductivity of the fluid
τ_{wx} **:** Wall shear stress along *x* - direction
τ_{wy} **:** Wall shear stress along *y* - direction
δ **:** Permeability parameter
α **:** Thermal diffusivity, (m^2 / s)
θ_w **:** Temperature ratio parameter
σ^* **:** Stefan-Boltzmann constant
λ **:** The fluid relaxation time
μ **:** Dynamic viscosity of the fluid
ρ_f **:** Density of the fluid (kg / m^3)

Superscript:

$/$ **:** Differentiation w.r.t η

Subscripts:

f **:** Fluid
w **:** Condition on the sheet
∞ **:** Ambient Conditions

ACKNOWLEDGMENTS

The authors express their gratitude to Dr. O. P. Pandey, the Chief Editor, for his insightful feedback and for editing the final manuscript. The authors are also thankful to reviewers for their comments and suggestions. No funding was received

Author Credit Statement

All authors have contributed equally. All authors have read and approved the manuscript

Data availability

On reasonable request, the datasets used and/or analyzed during the current investigation are accessible from the corresponding author, and all data created or analyzed during this study are included in this published publication.

Compliance with ethical standards

Declare no conflict of interest and adhere to copyright norms

REFERENCES

Babu, N.V.N., Gundagani, M. and Paul, A., 2015. Soret and Dufour effects on unsteady hydromagnetic free convective fluid flow past an infinite vertical porous plate in the presence of chemical reaction. J. Science and Arts, 15 (1), 99-111

Babu, N.V.N., Murali, G., Bhati, S.M., 2018. Casson fluid performance on natural convective dissipative couette flow past an infinite vertically inclined plate filled in porous medium with heat transfer, MHD and hall current effects. In. J. Pharmaceutical Res., 10(4), 809-819.

Deepa, G. and Murali, G., 2014. Effects of viscous dissipation on unsteady MHD free convective flow with thermophoresis past a radiate inclined permeable plate. Iranian J. Sci. Technology (Sciences), 38A3, DOI: 10.22099/IJSTS.2014.2437.

Deepa, G. and Gundagani, M., 2014.Analysis of soret and dufour effects on unsteady MHD flow past a semi infinite vertical porous plate via finite difference method. Int. J. Appl. phys. and math., 4(5), 332-344, DOI: 10.7763/IJAPM.2014.V4.306.

Farooq, U., Lu, D., Munir, S., Ramzan, M., Suleman, M. and Hussain, S., 2019. MHD flow of Maxwell fluid with nanomaterials due to an exponentially stretching surface, Scientific Reports. 9, 7312, doi: 10.1038/s41598-019-43549-0

Fetecau C. and Fetecau, C., 2003. A new exact solution for the flow of Maxwell fluid past an infinite plate. Int. J. Nonlin. Mech. 38(3), 423-427.

Fetecau, C., Athar, M. and Fetecau, C., 2014. Unsteady flow of a generalized Maxwell fluid with fractional derivative due to a constantly accelerating plate. Comput. Math. Appl. 57(4), 596-603.

Gundagani, M. and Babu, N.V.N., 2012. Effect of Radiation on MHD Convection Flow Past a Vertical Permeable Moving Plate**.** Int. J. Advances in Appl. Sci., (IJAAS)**,**1(1), 19-28.

Gundagani, M., Sivaiah, S., Babu, NVN. and Reddy, M.C.K. 2012. Finite element solution of thermal radiation effect on unsteady MHD flow past a vertical porous plate with variable suction. Int. J. Engineering & Techn., 1(3), DOI:10.14419/ijet.v1i3.52.

Gundagani, M, Sheri, S., Paul, A. and Reddy, M. C. K., 2013a. Unsteady magnetohydrodynamic free convective flow past a vertical porous plate, Int. J .Appl. Sci. and Engineering, 11 (3), 267–275

Gundagani, M., Sheri, S., Paul, A. and Reddy, M. C. K., 2013b. Radiation Effects on an Unsteady MHD Convective Flow Past a Semi-Infinite Vertical Permeable Moving Plate Embedded in a Porous Medium with Viscous Dissipation. Walailak J. Sci & Tech., 10(5), 499–515. DOI- 10.2004/wjst.v10i5.380

Gundagani, M., Babu, N.V.N., Gadially, D. et al., 2024a. Study of Nano-Powell-Erying fluid flow past a porous stretching sheet by the effects of MHD, thermal and mass convective boundary conditions. J. Umm Al-Qura Univ. Eng. Archit.,15, 271-281. https://doi.org/10.1007/s43995-024-00056-2,

Gundagani, M., Mamidi, L.P. and Tanuku, P.K., 2024b. Finite element solutions of Double diffusion effects on three-dimensional MHD Nano-Powell-Erying fluid flow in presence of thermal and mass Biot numbers. J. Eng. Appl. Sci., 71, Article 9 . https://doi.org/10.1186/s44147-023-00347-w

Haitao, Q. and Mingyu, X., 2007. Unsteady flow of viscoelastic fluid with fractional Maxwell model in a channel. Mechanics Res. Comm., 34(2), 210-212, https://doi.org/10.1016/j.mechrescom.2006.09.003.

Hayat, T. and Qasim, M., 2010. Influence of thermal radiation and Joule heating on MHD flow of a Maxwell fluid in the presence of thermophoresis. Int. J. Heat. Mass. Tran., 53 (21-22), 4780-4788.

Hayat, T., Abbas, Z. and Sajid, M., 2009. MHD stagnation point flow of an upper-convected Maxwell fluid over a stretching surface. Chaos. Soliton. Fract., 39(2), 840-849.

Heyhyat, M. M. and Khabazi, N., 2011. Non-isothermal flow of Maxwell fluids above fixed flat plates under the influence of a transverse magnetic field. Proc. Institution of Mechanical Engineers, Part C: J. Mech. Eng. Sci., 225, 909-916. doi:10.1243/09544062JMES2245.

Jamil, M. and Fetecau, C., 2010. Helical flows of Maxwell fluid between coaxial cylinders with given shear stresses on the boundary. Nonlin. Analy: Real. World. App. 11(5), 4302-4311.

Motsa, S. S., Hayat, T. and Aldossary, O. M., 2012. MHD flow of upper-convected Maxwell fluid over porous stretching sheet using successive Taylor series linearization method. J. Appl. Math. Mech., 33(8), 975-990.

Mukhopadhyay, S., De, P.R. and Layek, G.C., 2013. Heat transfer characteristics for the Maxwell fluid flow past an unsteady stretching permeable surface embedded in a porous medium with thermal radiation. J. Appl. Mech and Technical Phys. 54(3), 385-396.

Murali, G. and Babu, N.V.N., 2023. Convective MHD Jeffrey Fluid Flow Due to Vertical Plates with Pulsed Fluid Suction: A Numerical Study. J. Computational Appl. Mechanics, 54 (1), 36-48, DOI: 10.22059/ JCAMECH.2023.351326.773

Murali, G., Paul, A., and Babu, N.V.N., 2015a. Heat and mass transfer effects on an unsteady hydromagnetic free convective flow over an infinite vertical plate embedded in a porous medium with heat absorption. Int. J. Open Problems Compt. Math, 8 (1), 15-27.

Murali, G., Paul, A. and Babu, N.V.N., 2015b. Numerical study of chemical reaction effects on unsteady MHD fluid flow past an infinite vertical plate embedded in a porous medium with variable suction. Electronic J. mathematical analysis and appl.,3(2), 179-192,2015.

Murali, G., Deepa, G., Nirmala Kasturi, V. and Poornakantha, T., 2023. Joint effects of thermal diffusion and diffusion thermo on MHD three dimensional nanofluid flow towards a stretching sheet. Mathematical models in engineering, DOI: https://doi.org/10.21595/mme.2023.23590.

Mushtaq, A., Mustafa, M., Hayat, T. and Alsaedi, A., 2016. A numerical study for three-dimensional viscoelastic flow inspired by non-linear radiative heat flux. Int. J. Non-Linear Mechanics, 79, 83-87.

Qi, H. T. and Liu, J. G., 2011. Some duct flows of a fractional Maxwell fluid. The European Physical J. Special Topics, 193(1), 71-79, https://doi.org/10.1140/epjst/e2011-01382-6, 2-s2.0-79953717430.

Ramesh, G. K., Roopa, G. S., Gireesha, B. J., Shehzad, S. A. and Abbasi, F. M., 2017. An electro-magneto-hydrodynamic flow Maxwell nanoliquid past a Riga plate: a numerical study. J. Braz. Soc. Mech. Sci. Eng., 39, 4547-4554.

Reddy, M.K., Murali, G., Sivaiah, S. and Babu, N.V.N., 2012. Heat and mass transfer effects on unsteady MHD free convection flow past a vertical permeable moving plate with radiation. Int. J. Appl. Mathematical Res., 1 (2), 189-205. DOI:10.14419/ijamr.v1i2.45

Saleem, S., Awais, M., Nadeem, S., Sandeep N. and Mustafa, M. T., 2017.Theoretical analysis of upper-convected Maxwell fluid flow with Cattaneo-Christov heat flux model. Chinese J. Physics. https://doi.org/10.1016/j.cjph.2017.04.005.

Sandeep N. and Sulochana C., 2018. Momentum and heat transfer behaviour of Jeffrey, Maxwell and Oldroyd-B nanofluids past a stretching surface with non-uniform heat source/sink. Ain Shams Engineering J., 9(4), 517-524, https://doi.org/10.1016/j.asej.2016.02.008.

Singh, N., Kaur, J., Thakur, P., Murali, G., 2023. Structural behaviour of annular isotropic disk made of steel/copper material with gradually varying thickness subjected to internal pressure. Structural integrity and life, 23 (3), 293–297.

Sivaiah, S., Gundagani, M. and Karanamu, M. P., 2012a. Analysis of Heat and Mass Transfer Effects on an Isothermal Vertical Oscillating Plate. Walailak J. Sci. Tech., (WJST), 9(4), 407–415.

Sivaiah, S., Murali, G. and Reddy, M.C.K., 2012b. Finite Element Analysis of Chemical Reaction and Radiation Effects on Isothermal Vertical Oscillating Plate with Variable Mass Diffusion. Int. Scholarly Res. Network ISRN Mathematical Physics, Vol. 2012, Article ID 401515, doi:10.5402/2012/401515.

Sivaiah, S. , Muraligoud, G., Murali, G. and Reddy, M.C.K. ,2012c. Unsteady MHD mixed convection flow past a vertical porous plate in presence of radiation. Int. J. Basic and App. Sc., 1(4), 651-666, DOI:10.14419/ijbas.v1i4.106.

Sun, X., Wang, S. and Zhao, M., 2019. Oscillatory flow of Maxwell fluid in a tube of isosceles right triangular cross section. Phys. of Fluids, 31, 123101, https://doi.org/10.1063/1.5128764.

Tanuku, P. K. ., Mamidi, L. P. and Gundagani, M., 2024. Modelling and analysis of three-dimensional chemically reacting, radiating Casson-nanofluid flow: thermophoresis and Brownian motion effects. Acta Polytechnica, 64(5), 455–463. https://doi.org/10.14311/AP.2024.64.0455

Wang, Y. and Hayat, T., 2008. Fluctuating flow of Maxwell fluid past a porous plate with variable suction. Nonlin. Analysis: Real. World. Appl., 9(4), 1269-1268.

Wang, S. and Tan, W. C., 2011. Stability analysis of soret driven double-diffusive convection of Maxwell fluid in a porous medium. Int. J. Heat and Fluid flow, 32(1), 88-94.

Wang S., Li P. and Zhao M., 2019. Analytical study of oscillatory flow of Maxwell fluid through a rectangular tube, Phys. Fluids, 31, 063102, https://doi.org/10.1063/1.5100220.

Wenchang, T., Wenxiao, P. and Mingyu, X., 2003. A note on unsteady flows of a viscoelastic fluid with the fractional Maxwell model between two parallel plates. Int. J. Non-linear Mechanics,38(5), 645-650, https://doi.org/10.1016/s0020-7462(01)00121-4.

Zheng, L., Li, C., Zhang, X. and Gao, Y., 2011. Exact solutions for the unsteady rotating flows of a generalized Maxwell coaxial cylinders. Comput. Math. Appl., 62, 1105-1115

.

Received on: 12-05-2024; Revised on: 14-01-2025 ; Accepted on: 15-01-2025